Science Advances
AAAS

advances.sciencemag.org/cgi/content/full/6/20/eaaz6485/DC1

Supplementary Materials for

Topology control of human fibroblast cells monolayer by liquid crystal elastomer

Taras Turiv*, Jess Krieger, Greta Babakhanova, Hao Yu, Sergij V. Shiyanovskii, Qi-Huo Wei, Min-Ho Kim, Oleg D. Lavrentovich*

*Corresponding author. Email: tturiv@kent.edu (T.T.); olavrent@kent.edu (O.D.L.)

Published 13 May 2020, *Sci. Adv.* **6**, eaaz6485 (2020)
DOI: 10.1126/sciadv.aaz6485

The PDF file includes:

Supplementary Text
Sections S1 and S2
Figs. S1 to S10

Other Supplementary Material for this manuscript includes the following:

(available at advances.sciencemag.org/cgi/content/full/6/20/eaaz6485/DC1)

Movies S1 to S6

Supplementary Text

Section S1. Director field designs

Equation (1) in the main text shows how to produce director patterns with different charges of topological defects. We set $m\varphi = m_1 \arctan\left[y/\left(x+d_0/2\right)\right] + m_2 \arctan\left[y/\left(x-d_0/2\right)\right]$ for the pair of defects. The parameters present the concrete expressions and the director maps that correspond to the ones used to prepare substrates in Figs. 2-4.

- Pair of $-1/2$ and $+1/2$ defects: $m_1 = -0.5$, $m_2 = 0.5$, $d_0 = 1\,\text{mm}$ and $\varphi_0 = \pi/2$, for the pair with the director parallel to the line connecting two defect cores (Fig. S5A), or $\varphi_0 = 0$ for the pair with the director perpendicular to the line connecting two defect cores (Fig. S5B).
- Pair of -1 and radial $+1$ defects: $m_1 = -1$, $m_2 = 1$, $d_0 = 1\,\text{mm}$ and $\varphi_0 = 0$ (Fig. S5C).
- Pair of -1 and circular $+1$ defects: $m_1 = -1$, $m_2 = 1$, $d_0 = 1\,\text{mm}$ and $\varphi_0 = \pi/2$ (Fig. S5D).

Section S2. Dynamics of cells vs. fixed geometry of the liquid crystal elastomer (LCE) substrates

The dynamics of human dermal fibroblast (HDF) cells that manifests itself in splitting of integer strength defects into pairs of semi-integer defects and in in-plane motion of $+1/2$ defects described in the main text, Figs. 3,4, is the intrinsic feature of the living tissues that is not related to the potential evolution of the LCE substrate. The latter is fixed as specified by Eq. (1) and remains intact over the entire duration of the experiment. Figure S9 illustrate the statement by showing side-by-side images of the LCE substrate and of the tissue grown at this substrate. The LCE is imaged by polarized optical microscopy (POM); under POM, the cells are not visible. The tissue is imaged by phase contrast microscopy (PCM), which is not sensitive to light polarization. As clearly seen from co-localization of the textures, the dynamics of tissue defects is not associated with the dynamics of the LCE substrate.

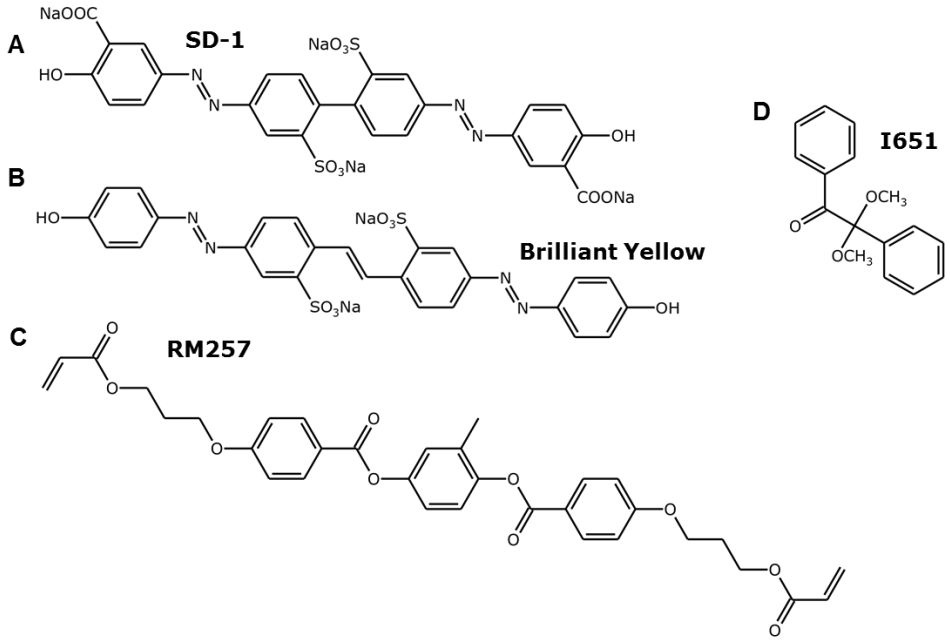

Fig. S1. Chemical structures of substances used. Chemical structure of (**A**) photoaligning azo-dye SD-1 and (**B**) Brilliant Yellow, (**C**) LCE diacrylate RM257 which is the main component of alignment layer for the tissues of HDF cells and (**D**) photoinitiator I651.

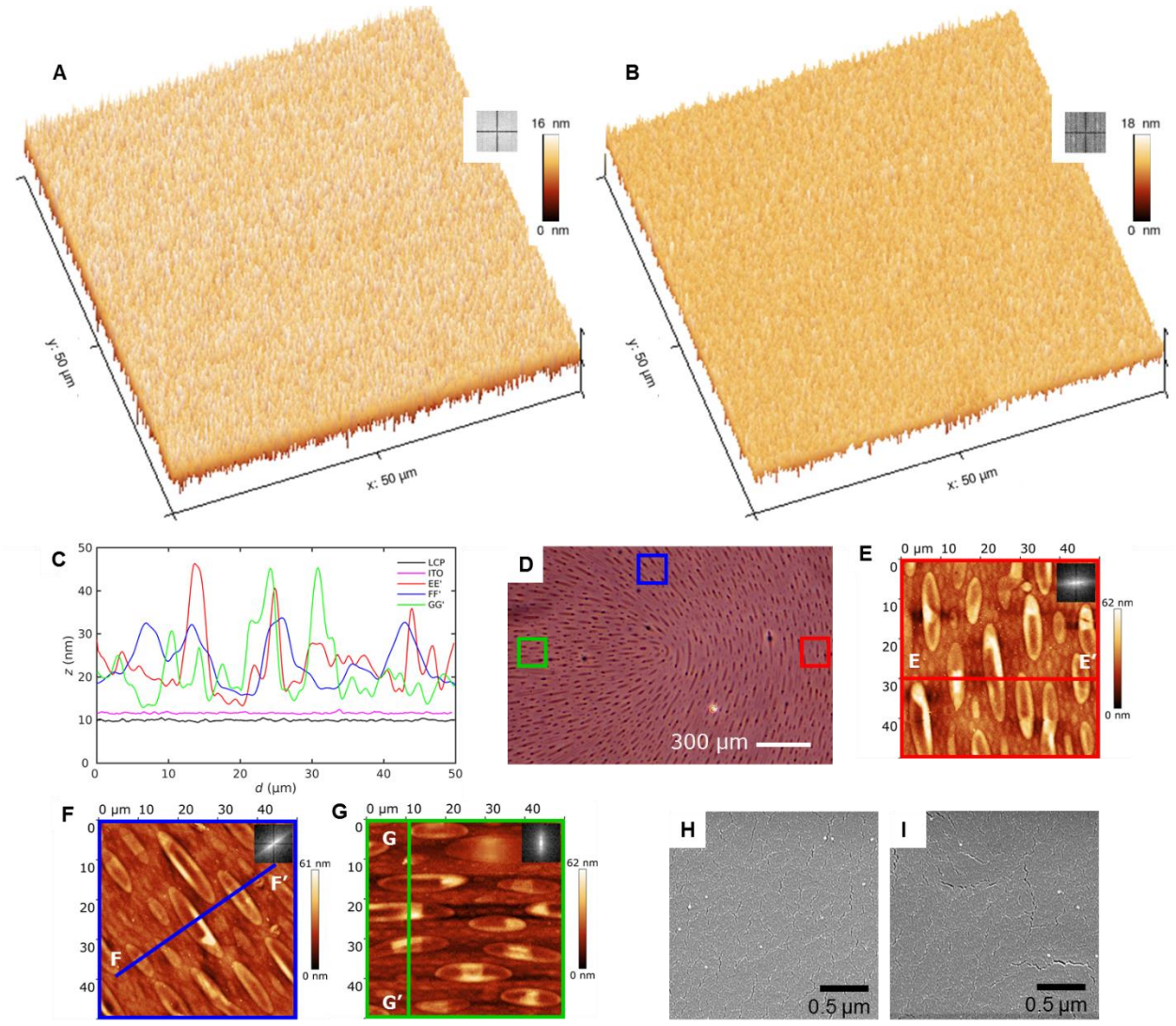

Fig. S2. Surface characterization of LCE and indium tin oxide (ITO) glass substrates. (**A**) LCE film with the uniform director along x-axis and (**B**) clean ITO glass before immersion into the cell culture medium. Insert textures represent 2D fast Fourier transformation of height map obtained from atomic force microscopy (AFM) with maximum spatial periodicity $0.5\,\mu m^{-1}$. (**C**) Profile of the surfaces before and after immersion. Surface profile taken along x-axis at $y = 12.5\,\mu m$ showing mean roughness of both LCE and ITO glass to be less than 2 nm. (**D**) Phase contrast microscopic image of patterned surface with topological defect $+1/2$ in LCE after the substrate was exposed to cell culture medium for 24 hours and dried for 3 hours at room temperature. (**E-G**) AFM scan of the substrate in (**D**) for different regions shown with red, blue and green squares. (**H-I**) Scanning electron microscopy of LCE substrates on (**H**) photoalignment azo-dye layer and (**I**) on clear ITO glass.

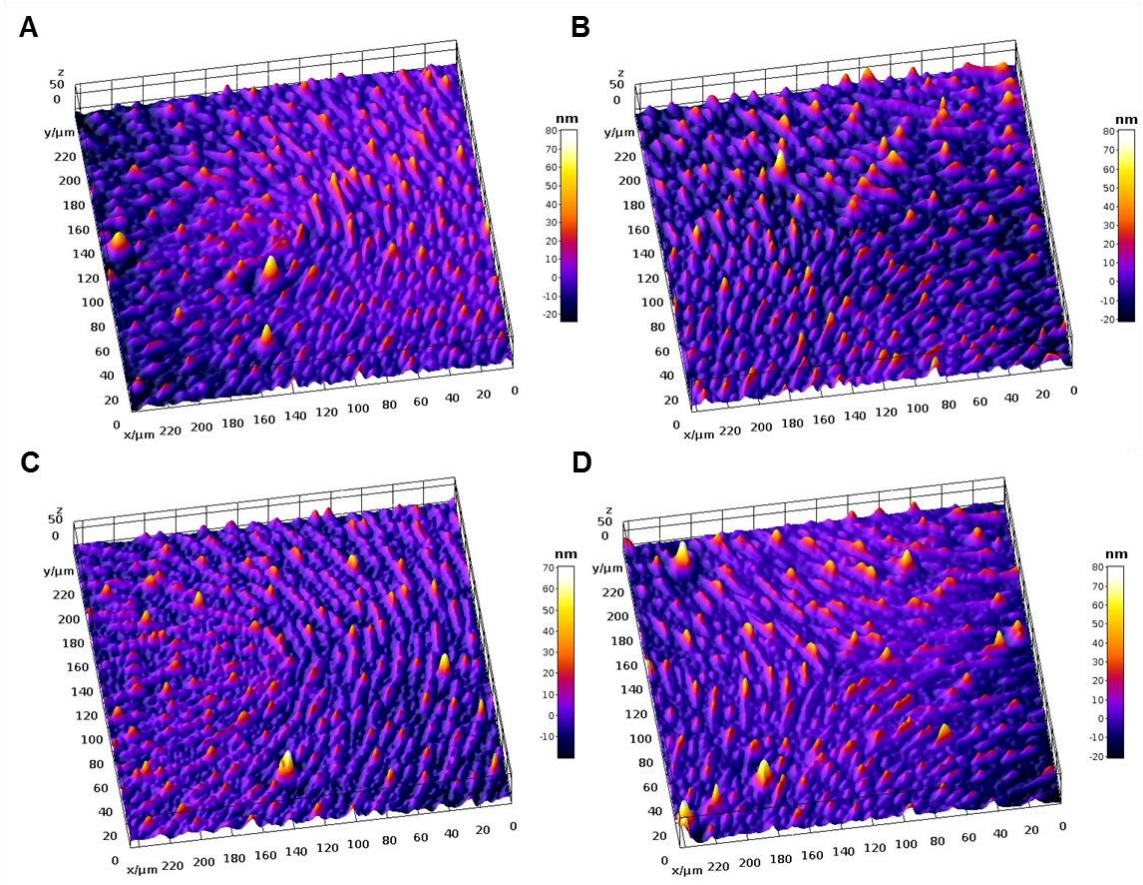

Fig. S3. Surface profile of patterned LCE after the cell culture medium immersion. (**A**-**B**) The surface profile of LCE developed after the substrate was immersed into the cell culture medium for 5 days obtained with digital holographic microscopy near (**A**) $+1/2$ and (**B**) $-1/2$ defects. (**C**-**D**) The surface profile of LCE after 14 days in the cell culture medium near similar (**C**) $+1/2$ and (**D**) $-1/2$ defects. All substrates were dried for 3 hours after exposure to cell culture medium.

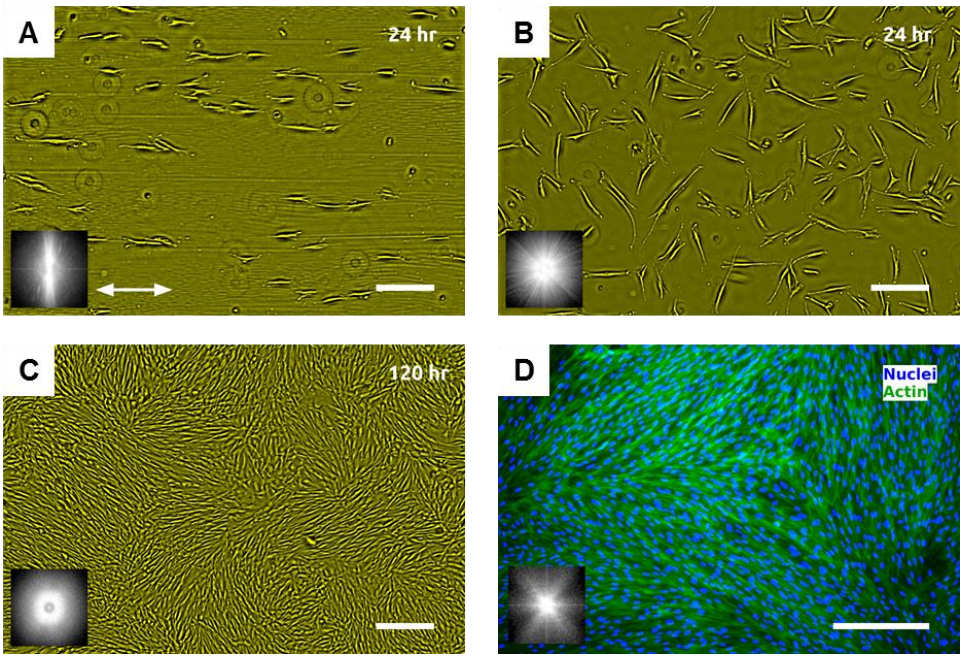

Fig. S4. HDF cells on LCE and ITO-glass substrates. (**A**-**C**) PCM textures of HDF cells growing (**A**) on LCE with the uniform director field along horizontal axis (white double-arrow) at 24 hours after seeding and (**B**-**C**) on a clean ITO glass substrate at (**B**) 24 hours (**C**) and 120 hours after seeding. Round shape objects in pictures (**A**) and (**B**) are cells in the suspension that are not yet adhered to the surface. (**D**) Fluorescent microscopy textures of the HDF tissue at confluency (240 hours), with fluorescently labeled nuclei (blue) and cytoskeleton F-actin proteins (green), grown at the ITO glass substrate. All scale bars are 300 μm.

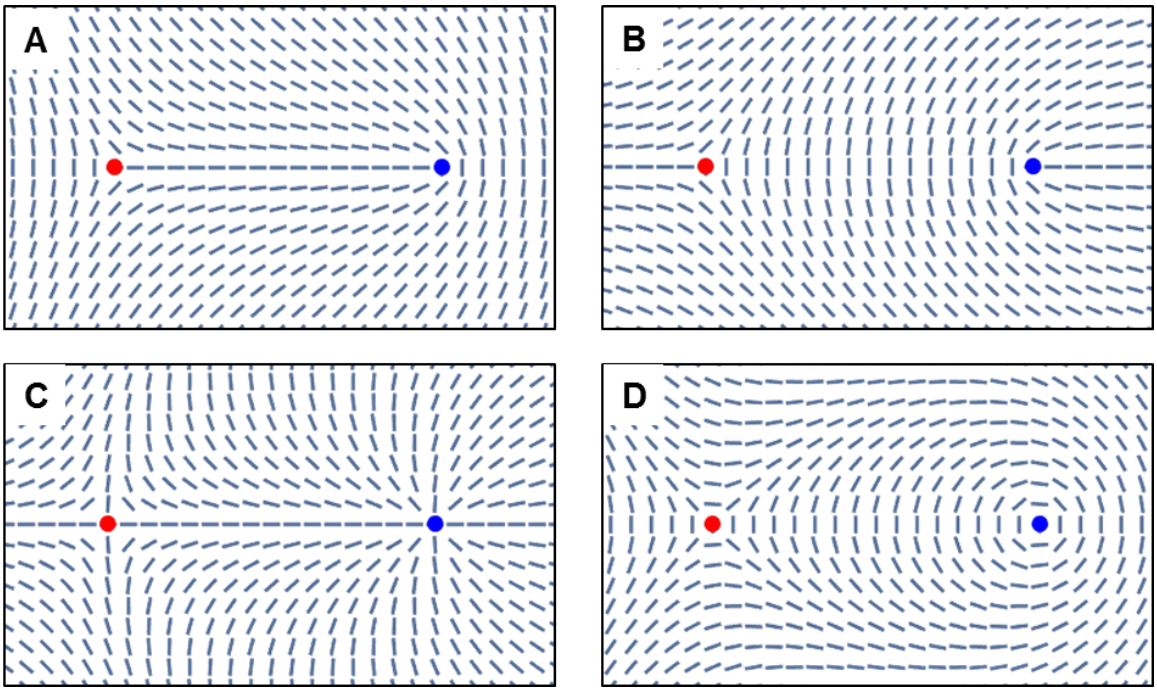

Fig. S5. The designed $\hat{\mathbf{n}}_{\mathrm{LCE}}$ containing topological defects. (**A**) Pair of $+1/2$ (blue disk) and $-1/2$ (red disk) defects with the director parallel to the line connecting them. (**B**) Pair of $+1/2$ (blue disk) and $-1/2$ (red disk) defects with the director perpendicular to the line connecting them. (**C**) Pair of radial type $+1$ (blue disk) and -1 (red disk) defects. (**D**) Pair of circular type $+1$ (blue disk) and -1 (red disk) defects.

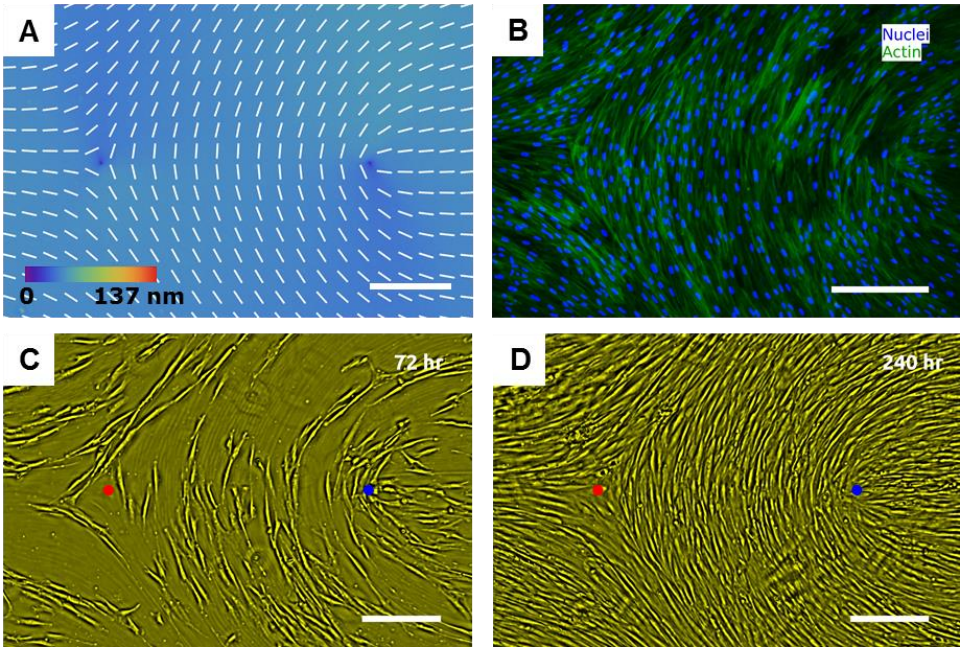

Fig. S6. HDF cells on LCE substrate patterned with pair of half-strength defects. (**A**) Director field of LCE obtained from PolScope. The director between the two defect cores is perpendicular to the line connecting them. (**B**) Fluorescently stained nuclei (blue) and cytoskeleton F-actin proteins (green) of the HDF cells. (**C**, **D**) PCM imaging of HDF cells proliferating on LCE at (**C**) 72 and (**D**) 240 hours of observation. Cells are seeded with the surface density 3.3×10^{7} m^{-2}. All scale bars are 300 μm.

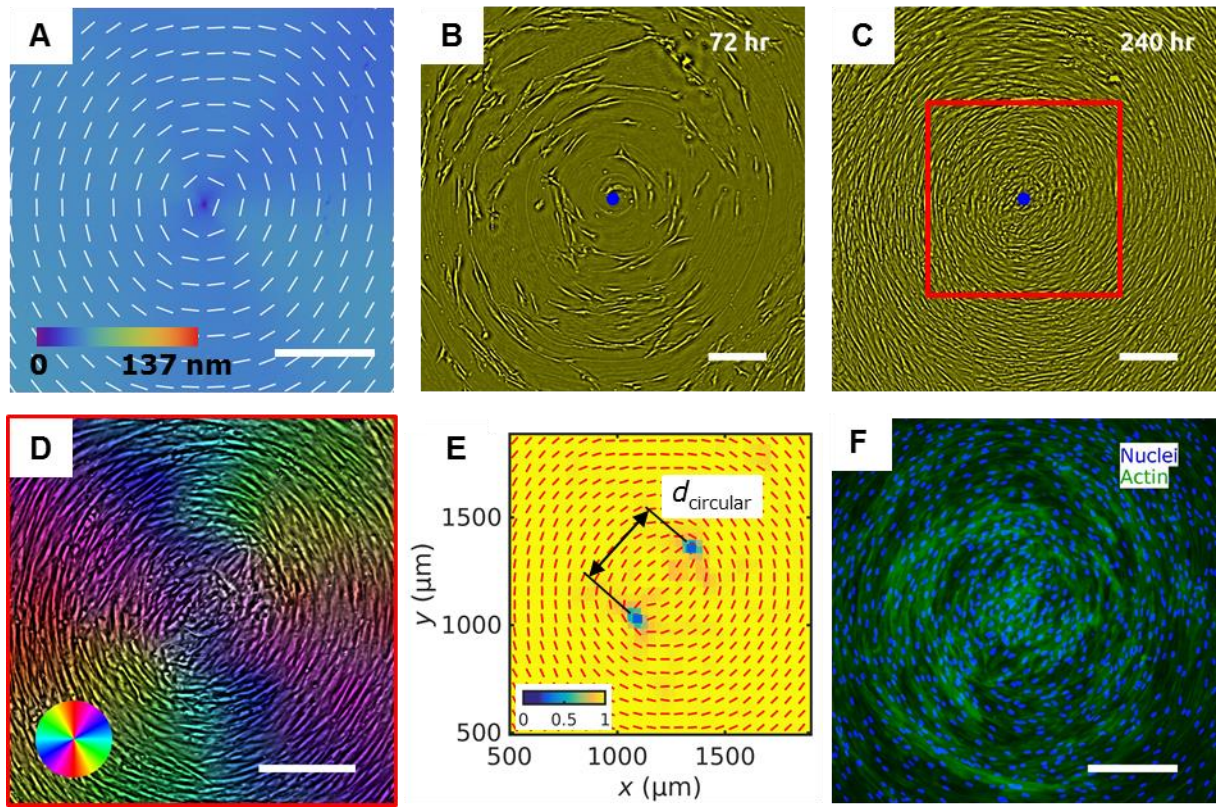

Fig. S7. HDF cells on patterned LCE substrate with +1 circular defect core. (**A**) Director field around +1 circular defect core of LCE obtained from PolScope. (**B**, **C**) PCM imaging of HDF cells growth at (**B**) 72 and (**C**) 240 hours after cells are seeded with the density 3.3×10^{7} m^{-2}. (**D**) Color-coded orientational field and (**E**) the corresponding scheme of patterned HDF tissue director $\hat{\mathbf{n}}_{HDF}$ obtained from local anisotropy of PCM texture inside the red frame in (**C**). Red bars in (**E**) denote local orientation of cells' long axes. The separation distance between two $+1/2$ defects near the +1 circular core $d_{circular} \approx 430\,\mu m$. (**F**) Fluorescent microscopy texture of stained nuclei (blue) and cytoskeleton F-actin proteins (green) of the HDF cells. All scale bars are 300 μm.

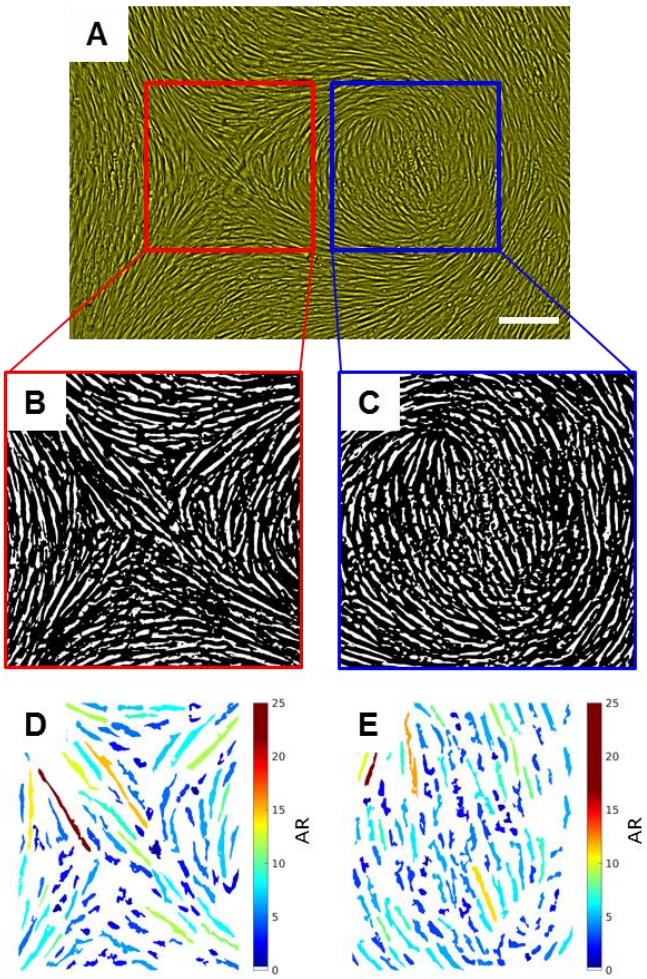

Fig. S8. HDF cells phenotypical differences near -1 and circular $+1$ defects pair. (**A**) PCM texture of the HDF cells. (**B**, **C**) Images of intensity thresholded PCM textures of the HDF cells grown near (**B**) -1 and (**C**) $+1$ defect. (**D**, **E**) Color-coded maps of intensity thresholded images showing the cells of different aspect ratio (AR). The average AR over all cells within the box of size $800\,\mu m$ near (**D**) -1 defect is 5.8 ± 2.7 and (**E**) $+1$ defect is 2.6 ± 1.5 (error is a standard deviation). The scale bar is 300 μm.

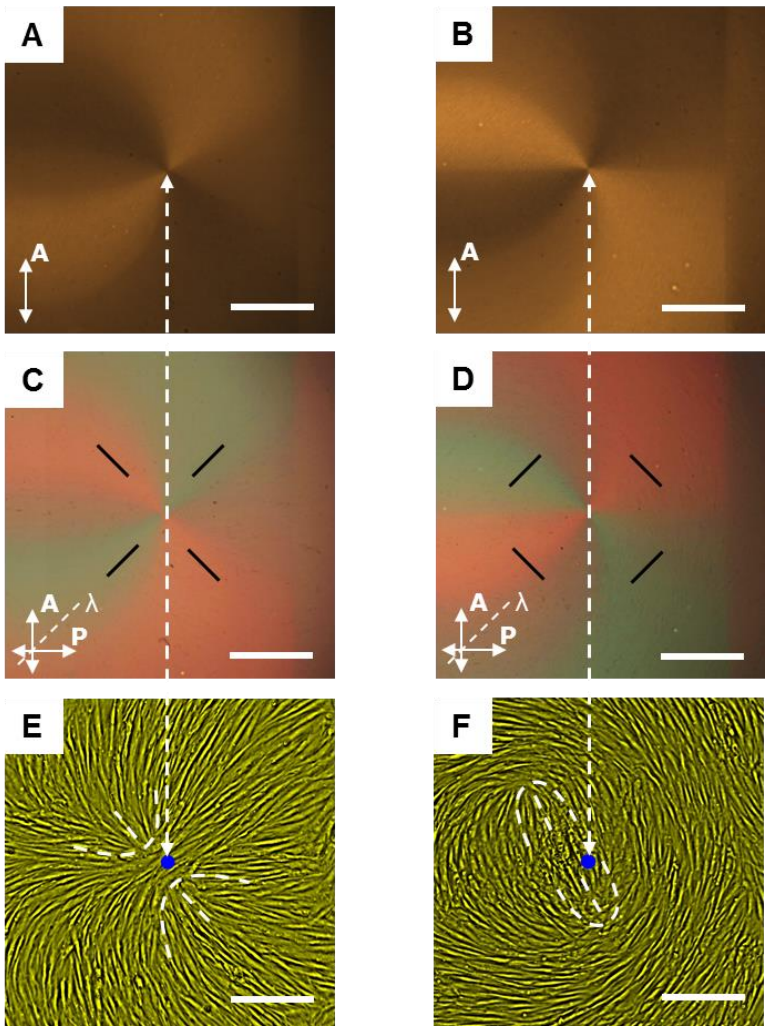

Fig. S9. Colocalization of topological defects in LCE with defects created in HDF cells. (**A**, **B**) POM textures of (**A**) +1 radial and (**B**) +1 circular type defects, image with analyzer inserted (polarization axis orientation is denoted by double-arrow line). The cores of the +1 radial and circular defects in the LCE substrate are seen as the convergence points of bright and dark brushes, pointed to by the white dashed double-arrow vertical lines. (**C**, **D**) POM texture of (**C**) +1 radial and (**D**) +1 circular type defects, image with polarizer, analyzer, and full-wave retardation plate inserted (the slow optical axis of the retarder is denoted with a dashed line). Black bars represent the orientation of the LCE director far from the defect core: blue-green color represents the optical retardation addition with the local $\hat{\mathbf{n}}_{\mathrm{LCE}}$ being parallel to the slow axis of the retarder and red-orange color regions represent local $\hat{\mathbf{n}}_{\mathrm{LCE}}$ that is perpendicular to the slow axis. (**E**, **F**) PCM textures of the HDF cells at 240 hours after seeding with the density of 3.3×10^{7} m^{-2} on LCE with (**E**) radial +1 and (**F**) circular +1 defect. Dashed white lines represent the local HDF cell orientation $\hat{\mathbf{n}}_{\mathrm{HDF}}$ with pairs of $+1/2$ defects. The blue disks in (**E**, **F**) represent the defects cores preinscribed in the LCE coating and colocalized with the HDF tissue textures. All scale bars are 300 μm.

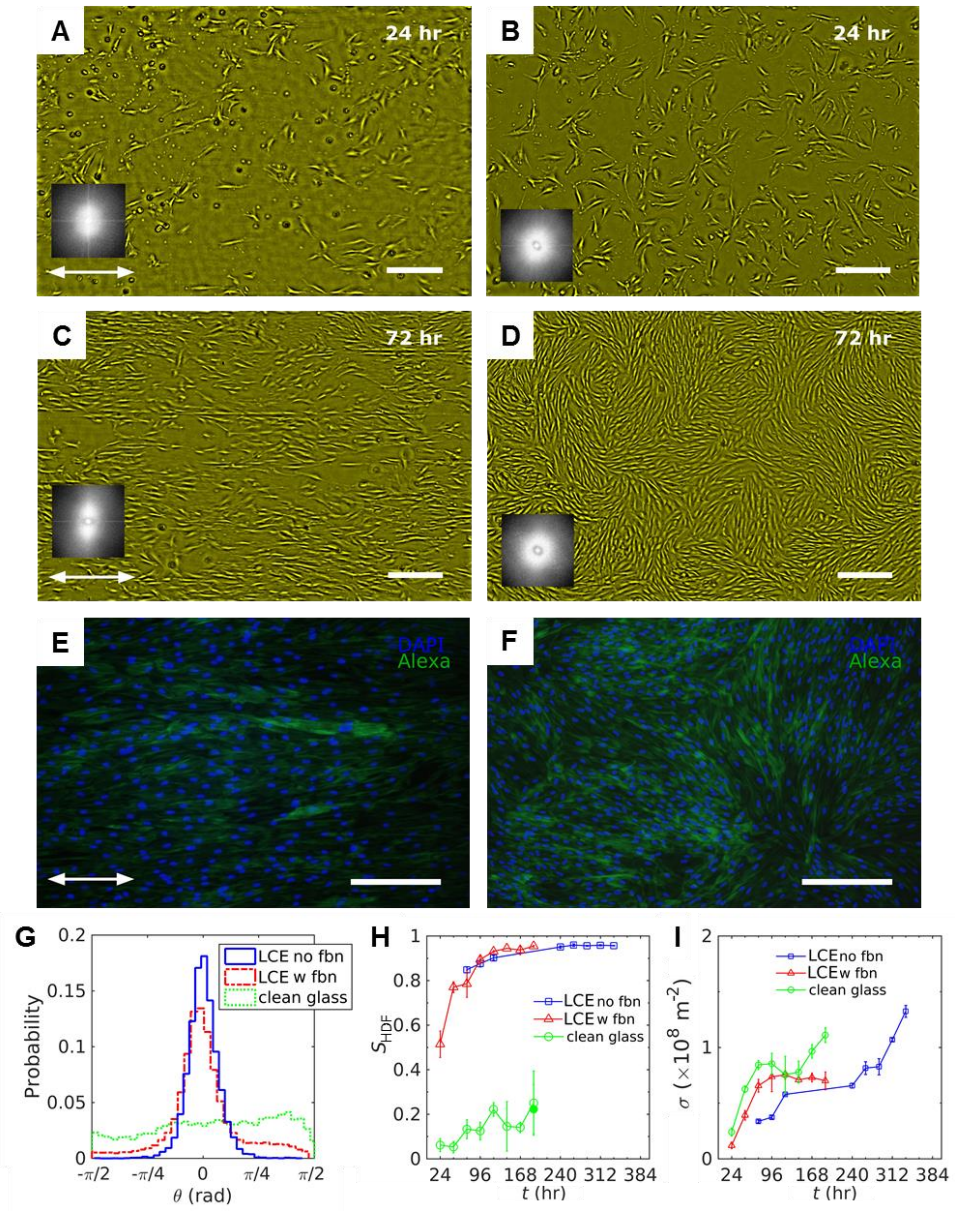

Fig. S10. HDF cells on substrates precoated with fibronectin. (**A**-**D**) PCM texture of HDF cells growth on (**A**) 24 and (**C**) 72 hours after cells seeding on LCE with uniform director field (indicated by white double-arrow) and at (**B**) 24 and (**D**) 72 hours after cells seeding on ITO glass. Both surfaces are precoated with fibronectin before cell seeding with the initial density of 3.3×10^7 m^{-2}. (**E**, **F**) Fluorescently stained nuclei (blue) and cytoskeleton F-actin proteins (green) of the HDF cells on (**E**) LCE and (**F**) ITO glass. (**G**) Distribution of the nuclei orientation. (**H**) Scalar order parameter S_{HDF} calculated from the cells' long axes orientation obtained from PCM textures. (**I**) Time evolution of the surface density of the HDF cells. All scale bars are 300 μm.